The influence of thermal maturity on the stable isotope compositions and concentrations of molybdenum, zinc and cadmium in organic-rich marine mudrocks

Alexander J. Dickson[1,2]*, Erdem Idiz[1], Donald Porcelli[1], Sander H.J.M. van den Boorn[3]

1. Department of Earth Sciences, University of Oxford, South Parks Road, Oxford, UK.
2. Department of Earth Sciences, Royal Holloway University of London, Egham, Surrey, UK.
3. Shell Global Solutions International B.V., Rijswijk, The Netherlands

*alex.dickson@rhul.ac.uk

Keywords: Molybdenum-isotopes, zinc-isotopes, cadmium-isotopes, organic matter, thermal maturity, pyrolysis

Abstract

The concentrations and isotopic compositions of molybdenum (Mo), zinc (Zn) and cadmium (Cd) in organic-rich marine mudrocks may be used to characterize ocean chemistry in the geological past. These approaches rely on the rarely tested assumption that the geochemical signatures of these metals are not affected by the thermal maturation of the organic matter with which they are associated. We have conducted a series of artificial maturation experiments on two well-known immature organic-rich mudrocks, the Kimmeridge Blackstone Band (Late Jurassic age), and the Posidonia Shale (Early Jurassic age). These pyrolysis experiments allow us to trace changes in the composition of organic matter through varying stages of maturation, and the concentration and isotopic compositions of metals in rock residues and evolved organic fluids. Our results indicate that the thermal maturation of organic matter does not result in significant alteration of the isotopic compositions of Mo, Zn and Cd in the rock residues, which thus retain primary palaeodepositional information. Systematic increases in the concentrations of Mo, Zn and Cd in rock residues with progressively higher thermal maturity are attributed to the loss of substrate mass in the form of fluids released during pyrolysis-induced cracking of kerogen, and to the relatively low concentrations of Mo, Zn and Cd in these fluids. The Mo-isotope compositions of fluids produced during pyrolysis are isotopically similar to the bulk rock; in contrast the isotopic composition of Zn in organic fluids is ~0.4–0.6 ‰ lighter than the bulk rock. The progressive loss of organic matter from rock residues during maturation coupled with the increases in metal concentrations leads to an increase of metal/TOC ratios, which may be up to double their original (syn-depositional) value in thermally mature rocks. This observation must be taken into account when using metal/TOC ratios as proxies for oceanic metal inventories throughout geological time. Finally, calculations using the mass of asphaltenes recovered during the pyrolysis experiments suggest that organically bound Mo, Zn and Cd account for several percent of the total rock metal inventory.

1. Introduction

Sedimentary organic matter (kerogen) is thermally degraded during the process of catagenesis (Tissot and Welte, 1984). With progressive burial, kerogen undergoes thermal cracking in response to increasing temperature (typically on the order of ~30^{o}C heating per kilometer of burial) resulting in the production of lower molecular weight compounds in a solvent-extractible bitumen fraction (Fig. 1). In the early stages of cracking, this bitumen is composed of a significant proportion of high molecular weight asphaltenes that contain N, S and O heteroatoms, and are generally accepted as smaller building blocks of the parent kerogen. With progressive maturation, more of the kerogen is cracked to generate bitumen, which itself undergoes further cracking as well as disproportionation, generating lower molecular weight hydrocarbon molecules and a coke-like C-rich residue that is insoluble (pyrobitumen). During this process, there are also losses of gases such as CO_2, H_2O and H_2S. Overall, as kerogen becomes more thermally 'mature,' it passes through the stages of oil generation and gas generation, with up to 60% of the original organic matter lost due to secondary migration of the generated products away from the host rock (Tissot and Welte, 1984; Lewan et al., 1979; Raiswell and Berner, 1987). The end of the maturation process (metagenesis) comprises a C-rich residue from the original kerogen and pyrobitumen (coke) from secondary cracking and disproportionation of bitumen.

Trace metals in organic-rich rocks

Some metals are found in high concentrations in organic-rich rocks (e.g. Brumsack et al., 1980). These enrichments can be attributed to low Eh conditions in aquatic environments that promote the delivery and burial of organic-matter and redox-sensitive metals such as Mo, U, V, Ni, Cd, Zn, Cr and Re (Tribovillard et al., 2006; Piper and Calvert, 2009). Relationships between these metals and between metals and total organic carbon (TOC), have been used to define indices to reconstruct paleoenvironmental conditions during the deposition of marine sediments (e.g. Lewan and Maynard, 1982; Lewan, 1984; Algeo and Lyons, 2006; Algeo and Tribovillard, 2009; Sweere et al., 2016).

Metals associated with organic-matter in sedimentary deposits may be adsorbed or bound by organic ligands in compounds such as metalloporphyrins, naphthenates, metal chlorins, or high-molecular weight polar compounds (e.g. asphaltenes) (Filby, 1994). For example, Ni and V are known to be incorporated into organic porphyrins under specific Eh–Ph conditions (Lewan and Maynard, 1982, Lewan, 1984), and have the highest concentrations of metals in oils and bitumens (Ellrich et al., 1985; Mercer et al., 1992; Fitzgerald and Filby, 1992). Other metals have also been measured in oils and bitumens at µg/g concentrations, although it is not clear how these metals are structurally associated with the organic matter (e.g. Ellrich et al., 1985; Odermatt and Curialle, 1991; Mercer et al., 1992; Fitzgerald and Filby, 1992; Selby et al., 2007). Direct measurement of metal bound to kerogen is difficult as the only way to isolate kerogen is by destroying the mineral matrix through the use of strong acids such as HF and HCL, which can also affect the metal

content of the kerogen. Consequently the behaviour of metals in organic-rich mudrocks as bitumen is generated and removed from the parent kerogen is poorly understood.

Metals and metal isotopes as palaeo-chemical tracers

The isotopic compositions of molybdenum, cadmium and zinc in organic-rich marine sediments have recently been investigated as tracers for redox conditions and nutrient cycling in past oceans (Georgiev et al., 2015; Little et al., 2016; Vance et al., 2016; Dickson, 2017; Kendall et al., 2017). Implicit in these studies is the assumption that changes in the structure of the organic matter to which these metals may be bound, nor the progressive loss of organic matter during thermal maturation and fluid migration, will affect the isotopic composition of the bulk rock. This assumption is important, because the behaviour of these metal-based isotope systems are defined from observations of waters and sediments accumulating in the modern ocean, where thermal maturation is unimportant (Barling et al., 2001; McManus et al., 2002; Neubert et al., 2008; Siebert et al., 2003, 2006; Poulson et al., 2006; Poulson-Brucker et al., 2009; Noordman et al., 2014; Little et al., 2016; Vance et al., 2016). In contrast, many studies, particularly using the molybdenum-isotope system, use organic-rich mudrocks from the geological record that have undergone varying degrees of burial and uplift, and hence, thermal maturation (e.g. Arnold et al., 2004; Wille et al., 2008; Duan et al., 2010; Gordon et al., 2010; Asael et al., 2013). While some studies (Mongenot et al., 1996; Ardakani et al., 2017) have suggested that thermal maturation may have little influence on the concentration of molybdenum in organic-rich mudrocks, there is no current evidence for the effect of maturity on the isotopic composition of transition metals.

This study uses controlled laboratory pyrolysis experiments to determine whether thermal maturation leads to discernable shifts in the isotopic composition and concentration of molybdenum, cadmium and zinc in organic-rich mudrocks. Furthermore, we investigate the partitioning of these metals between organic sub-fractions by measuring the concentration and isotopic compositions of metals in the solvent-extractable organic matter (bitumen) and the fraction of this bitumen that is insoluble in apolar solvents (asphaltenes). The metal concentrations within the asphaltene fractions are subsequently used to calculate the inventory of organically-bound metals in the bulk rocks.

2. Methods

Artificial maturation of kerogen using pyrolysis is commonly utilized to simulate the hydrocarbon generation process (Lewan, 1979; Lewan et al. review). In this study, a series of aliquots of two thermally immature organic-rich mudrocks were pyrolysed for varying lengths of time at a fixed temperature of 325^{o}C. Operational terms for each sample fraction are noted in Fig. 2 and used throughout the discussion, but are briefly noted here for clarity. *Bulk rocks* are the unaltered, powdered rock without any additional chemical treatment; *extracted rock residues* are rock powders from which soluble organic matter has been removed; *bitumen* is the total soluble organic

matter; *asphaltenes* are the high-molecular weight bitumen fraction that is insoluble in *n*-heptane; and *maltenes* are the hydrocarbon-containing lighter molecular weight bitumen fraction that is soluble in *n*-heptane. Bitumen that evolved at each step of the pyrolysis process was extracted using organic solvents, and the concentrations and isotopic compositions of Mo, Zn and Cd were measured from these and the extracted rock resides.

2.1 Sample material

Two samples were used in this study. The first was obtained from the Blackstone Band level of the Kimmeridge Clay Formation (Late Jurassic age), exposed in outcrop in Kimmeridge Bay, Dorset, England. The organic matter in this outcrop is immature, with a low vitrinite reflectance (VR%) of ~0.4–0.5 (Scotchman, 1990). The second sample was obtained from the carbonate-rich Posidonia Shale (Early Jurassic age) in a drill core taken from the Lower Saxony Basin (LSB) in northern Germany. The sample used is also immature, with a VR% of ~0.54. Large (200 g) aliquots of each sample were carefully cleaned to remove external surfaces and homogenized in an agate TEMA mill.

2.2 Preparation of labware, acids and solvents

Laboratory reagents, glassware and Teflon were treated prior to use to remove organic and inorganic contaminants. Teflon labware was refluxed in concentrated HNO_3 and soaked in dilute HCl, HNO_3 and ultra-pure (18.2 MΩ) water. Glassware was initially sterilized at 450^{o}C in a furnace overnight before soaking in hot 20% HNO_3 and rinsed with hot 18.2 MΩ water. Trace-metal-grade acids were quartz-distilled prior to use. All organic solvents (*n*-heptane, methanol (MeOH), dichloromethane (DCM)) were purchased as HPLC or trace-metal grade, and subsequently distilled in a Teflon u-bend still to further reduce the level of metal contaminants. Most chemical steps were undertaken in a class 10 trace-metal-clean laminar flow hood. However, Soxhlet extractions were undertaken in a pre-cleaned standard laboratory fume hood. Soxhlet thimbles were acid-cleaned PTFE.

2.3 Pyrolysis experiments

The experimental approach used is summarized in Fig. 2. Untreated aliquots of the Kimmeridge Clay and Posidonia Shale were analysed for bulk organic and inorganic geochemical characteristics (outlined in sections 2.4 and 2.5). Indigenous bitumen was then extracted from ~10 g sub-samples using a 3:1 mixture of DCM:MeOH in a Soxhlet for 36 hours. The extracted rock residues were dried, re-homogenized and subdivided into 1.5 g aliquots, which were loaded into clean glass Carius tubes. Each Carius tube was connected to a vacuum extraction line and flame sealed after the internal pressure was reduced to 10^{-2} atm. The tubes were then loaded into stainless steel containment vessels for heating.

Each sample was subjected to isothermal heating at 325°C for either 1 day, 4 days, 2 weeks or 5 weeks. Upon removal from the furnace, Carius tubes were taken from their stainless steel jackets and immediately placed in a freezer set to -80°C. Each tube was scored with a diamond cutter and broken open. Any bitumen evolved during pyrolysis heating was then extracted by Soxhlet refluxing for 36 hours. The remaining extracted rock residues were dried and re-homogenised prior to characterisation of their bulk organic and inorganic geochemistry.

The bitumen fractions were dried under a stream of N_2 and then weighed to obtain their dry mass. After an aliquot was taken for ICP analysis, each sample was mixed with 5–10 ml *n*-heptane, agitated for 30 minutes, and left to settle overnight. This process separated the high-molecular-weight asphaltene fraction. The remaining maltene fraction was removed from the precipitated asphaltenes by pipette after centrifugation. The asphaltene residues were treated with a further *n*-heptane rinse to ensure complete maltene removal. Both fractions were dried gently on a hotplate at 35°C and the dry residues were weighed.

2.4 Bulk organic geochemistry

The amount, composition and thermal maturity of the organic matter in the extracted and unextracted bulk rocks and rock residues were characterized using a Rock-Eval 6 (Behar et al., 2001). Samples were measured in triplicate and the precision of the measurements was monitored using 13 analyses of an in-house mudrock standard (St. Audries Bay Shale). The relative 2 S.D. precisions were ±6 % for total organic carbon (TOC), ±10 % for hydrogen index, and ±0.5 % for $T_{max.}$ Note that T_{max} is the temperature of maximum hydrocarbon generation during the Rock-Eval analysis and is an indicator of thermal maturity. It is not the same as the temperature the samples were heated to during pyrolysis in section 2.3. Individual uncertainties are shown in Fig. 3 as the 2 S.D. of triplicate measurements for each sample.

2.5 Inorganic geochemistry

For metal concentrations, sample aliquots were digested in a 3:1 mixture of concentrated HNO_3 and HCl for 3 days to oxidize organic matter and authigenic components, and were subsequently dried and re-dissolved in 2:1 HNO3/HF to dissolve silicates. Sample digests were diluted 7500-fold and measured on a quadrupole ICP-MS. The accuracy and precision of trace-metal concentration data were monitored using standards within each run, and were within ±10% for Mo, Cd and Zn.

Isotopic measurements of Mo and Zn were made from the same sample powder aliquot. An aliquot containing ~400–500 ng Mo and Zn was mixed with purified solutions containing a ^{100}Mo–^{97}Mo double spike and a ^{67}Zn–^{64}Zn double spike. Double spikes were added so as to obtain a spike to sample ratio for Mo of ~0.6, and a spike to sample ratio for Zn of ~1.2. Samples were digested initially in inverse *aqua-regia* at 150°C for 48 hours. Subsequently, a small amount of HF was added to dissolve silicates and heated for 24 hours at 120°C. Following digestion, Mo and Zn were separated using a 200 µl anion-exchange column (Sweere et al., 2018). The Zn aliquot was

passed through the column procedure a second time to maximize the removal of interfering elements Ba and Ni. Similar procedures were used to purify Mo and Zn from the bitumen and asphaltene extracts, except that double spikes were added directly to the digested sample aliquots previously used for quadrupole ICP-MS measurements.

The bulk rock and extracted rock residue digests initially used for quadrupole ICP-MS measurements were spiked with a ^{113}Cd–^{111}Cd double spike to obtain a spike/sample ratio of ~1. Cd was purified from matrix elements using 2 ml AG1-X8 anion exchange resin (200–400 mesh). Samples were loaded in 0.5M HCl/1M HF, and matrix elements were subsequently washed off in 0.5M HCl/1M HF and 4M HCl. Sn was then eluted in 10 ml 3M HNO_3/0.1M HBr, before Cd was eluted in 8 ml 3M HNO_3. The column procedure was then repeated using 200 µl columns to ensure removal of the inferring element Sn. Samples were loaded in 0.8 ml 0.5M HCl/1M HF, and matrix elements were removed with 1.5 ml 0.5M HCl/1M HF and 1.5 ml 4M HCl. Sn was eluted in 1.2 ml 3M HNO_3/0.1M HBr, before Cd was eluted in 1 ml 3M HNO_3. Cd recovery was typically >95%.

Isotopic measurements were made using a Nu Plasma I MC-ICP-MS coupled to a Nu Instruments DSN desolvating sample introduction system. Mo- and Cd-isotopes were measured on ~80 ppb and 60 ppb solutions respectively in low-resolution mode. Zn isotopes were measured on ~120 ppb solutions in medium-resolution mode. To account for changing backgrounds in the instrument, blank 2% HNO_3 acid was measured prior to every sample and subtracted from the raw sample voltages before data processing. All samples were corrected to bracketing isotopic standard solutions mixed with a similar proportion of double-spike. Spike-sample mixtures were re-processed from the raw voltage data offline, and the results are expressed in delta-notation as follows:

$$\delta_{Mo,\,Cd,\,Zn} = ((R_{sample} - R_{standard}) / R_{standard}) * 1000 \quad (1)$$

Where R is either the $^{98}Mo/^{95}Mo$, $^{66}Zn/^{64}Zn$, or $^{114}Cd/^{110}Cd$. Mo isotopes are expressed as $\delta^{98/95}Mo$ relative to NIST 3134, where NIST 3134 has a value of +0.25 ‰ (Nägler et al., 2014). Zn isotopes are expressed as $\delta^{66/64}Zn$ relative to IRMM-3702, where IRMM-3702 has a value of +0.28 ‰ (Archer et al., 2016). Cd isotopes are expressed as $\delta^{114/110}Cd$ calculated using the composition NIST 3108 as the standard (Abouchami et al., 2012). Mo, Zn and Cd concentrations were calculated by isotope dilution, using the $^{100}Mo/^{95}Mo$, $^{64}Zn/^{66}Zn$ and $^{111}Cd/^{112}Cd$ ratios.

The accuracy and reproducibility of the Mo data was estimated using repeated digestions of the SDO-1 USGS shale standard, which gave a value of 1.04 ± 0.08 ‰ (n = 33, 2 S.D.) that is within uncertainty of the value published by Goldberg et al. (2013). The accuracy and precision of Zn and Cd measurements were assessed using measurements of the AA-ETH Zn (Alfa Aesar Zn foil, lot I17Z058) solution standard and the ‘OxCad’ (Alfa Aesar Specpure Cd, lot 81-081192A) Cd solution standards, spiked and diluted in proportion to ‘unknown’ samples measured in the same analysis sessions. The reproducibility of Zn and Cd measurements was also estimated with a

limited number of SDO-1 digestions. The value measured for AA-ETH was 0.04 ± 0.11 ‰ relative to IRMM-3702 (n= 13, 2 S.D.), which is within uncertainly of the weighed mean of -0.02 ± 0.032 ‰ published by Archer et al. (2016). The 2 S.D. reproducibility of $\delta^{66/64}$Zn for SDO-1 was ± 0.07 ‰ (n = 7). The value measured for OxCad was -0.86 ± 0.06 ‰ (n = 9, 2 S.D.), which is within uncertainty of the value of -0.81 ± 0.1 ‰ published by Abouchami et al. (2012). The 2 S.D. reproducibility of $\delta^{114/110}$Cd for SDO-1 was ± 0.06 ‰ (n = 5).

A procedural blank was measured by refluxing distilled organic solvents in a clean Soxhlet for 36 hours. These solvents were transferred to a Teflon vial and evaporated dry, before being digested using the same mixture of HNO_3, HCl and HF as the bulk sediment samples. After evaporating the digestion acids, the sample was re-diluted in 10ml 2% HNO_3 and measured using a quadrupole ICP-MS in the same analysis session as the bulk sediment powders. The total procedural blanks for Mo and Zn were 2 ng and 8 ng respectively, which are <0.5% of the total Mo and 1–2% of the total Zn processed per sample. The Cd blank was below the detection limit.

3. Results

3.1 Bulk organic geochemistry

Results of the bulk organic geochemical measurements are shown in Fig. 3 and Tables 1 and 2. As expected, the effect of progressively longer pyrolysis heating results in increasing maturation of both samples. The Rock-Eval T_{max} (temperature of maximum hydrocarbon yield) over the course of the 1 day, 4 day, 2 week and 5 week experiments increased from 413 to 450^{o}C (equivalent to a calculated vitrinite reflectance (VR/E%) of ~0.4–1.0, with the vitrinite equivalence calculated from T_{max}) for the Kimmeridge Clay and 432 to 450^{o}C (VR/E% of ~0.54–1.0) for the Posidonia Shale. Correspondingly, TOC decreased from 35% to 29% (-17% change) for the Kimmeridge Clay and from 13% to 7% (-42% change) for the Posidonia Shale. The hydrogen index (HI) decreased from 733 to 178 mgHC/g TOC for the Kimmeridge Clay and from 702 to 239 mgHC/g TOC for the Posidonia Shale. The decreases in HI are represented as near linear increases in the transformation ratio (TR) of both rocks with progressive longer heating times (Fig. 3). These results are consistent with primary cracking of the kerogen and production of bitumen (and gas) during catagenesis, with linear relationships between heating time and T_{max}, HI, TOC and TR (Fig. 3).

The highest maturity sample for the Kimmeridge Clay does not contain the lowest TOC concentration of the experiments. This observation suggests at the highest maturities, disproportionation of bitumen into pyrobitumen (coke) and lighter hydrocarbons and gases occurred, resulting in increased TOC in the rock residues as a result of the addition of unextractable organic mater.

3.2 Trace metal concentrations of bulk rocks and extracted rock residues

Mo, Zn and Cd concentrations and isotope ratios for bulk rocks and extracted rock residues are shown in Fig. 4, and in Tables 1 and 2. The bulk rock Mo concentrations of 47 ppm for the

Kimmeridge Clay and 124 ppm for the Posidonia Shale represent significant authigenic enrichments of >150-fold above average crustal values when normalized to Al. The results of the pyrolysis experiments show that Mo concentrations increase across the maturity range, from 47 to 74 ppm for the Kimmeridge Clay and 124 to 132 ppm for the Posidonia Shale. Mo/TOC ratios calculated for each rock increase by ~58–85% over the same maturity range. The bulk rock Zn concentrations of 42 ppm for the Kimmeridge Clay and 211 ppm for the Posidonia Shale also represent authigenic enrichments of ~2.5 for the Kimmeridge Clay and ~10 for the Posidonia Shale when normalized to Al. For the Kimmeridge Clay, the Zn concentration is ~37 ppm in the bulk rock, while extracted rock residues have higher values of ~55 ppm, with one outlier of 117 ppm. For the Posidonia Shale, Zn concentrations for the bulk rock and non-pyrolysed rock residue are 243 and 195 ppm, respectively. The difference can potentially be explained by a significant adsorbed Zn component that was removed during solvent treatment. The Zn concentration of the extracted rock residue after 4 days of heating has a higher value of 293 ppm Zn. The bulk rock Cd concentrations of 1 ppm for the Kimmeridge Clay and 2.6 ppm for the Posidonia Shale are enriched >380-fold above average crustal values when normalized to Al. Cadmium concentrations behave in a similar manner to molybdenum, increasing across the maturity range from 1 to 1.4 ppm for the Kimmeridge Clay and from 2.4 to 3.1 ppm for the Posidonia Shale (Fig 4). Cd/TOC ratios increase across the maturity range by ~45% for the Kimmeridge Clay and by 105% for the Posidonia Shale.

3.3 Trace metal concentrations of bitumens and asphaltenes

The Mo and Zn concentrations and isotope compositions of extracted bitumens and asphaltenes are shown in Fig 5 and Tables 1 and 2. Although these concentrations are appreciable, they are significantly lower than in the bulk rock starting materials and the extracted rock residues. For the Posidonia Shale, bitumens and asphaltenes have up to 32 ppm Mo, which is lower than the rock residues. Similarly, the concentrations of Zn in the bitumens and asphaltenes are generally <33 ppm, with a single much higher value of 93 ppm. Interestingly, the Mo/Zn ratio in the extracted rock residues are in the 0.9–1.2 range, but are ~0.4 in the bitumens (Tables 1 and 2). These ratios suggest that a greater fraction of Zn is mobilized in the bitumen phase compared to Mo, with the implication that a significantly larger proportion of the total Zn is bound or adsorbed to kerogen than total Mo.

The Mo and Zn concentrations for the Kimmeridge Clay bitumens are similar to those of the asphaltenes (Fig. 6). Mo and Zn are both slightly more concentrated in the asphaltene versus the bitumen fractions of the Posidonia Shale. The ICP-MS analyses of Cd concentrations averaged 0.12 ppm for Kimmeridge bitumens and 0.11 ppm for Posidonia bitumens.

3.4 Trace element isotope compositions

For the bulk rocks, as well as the extracted rock residues, the Mo, Zn, and Cd isotope ratios are indistinguishable across the full maturity range for both the Kimmeridge and Posidonia samples

(Fig. 4). The average bitumen $\delta^{98/95}$Mo values for the Kimmeridge samples are similar to the bulk rocks and rock residues, albeit with a greater spread in the data (Fig. 5). Posidonia shale bitumen $\delta^{98/95}$Mo values are marginally lighter than the bulk rock and rock residues (average [residue – bitumen] = 0.27 ‰). For $\delta^{66/64}$Zn, the average [extracted rock residue – bitumen] difference is 0.4–0.6 ‰, which is the same range as the difference between the isotopic composition of modern seawater and Zn accumulating in organic-rich sediments (Little et al., 2016; Vance et al., 2016). The Mo and Zn isotope compositions of bitumens and asphaltenes are almost identical to one another in both the Kimmeridge Clay and Posidonia Shale (Fig. 6). The total mass of Cd recovered in the bitumen extracts was insufficient for isotopic analysis.

4. Discussion

4.1 Isotope compositions of rock residues

The most striking feature of the isotope data is the lack of variability in the fractions that have undergone different levels of pyrolysis for both the Kimmeridge and Posidonia samples (Fig. 3), despite a loss of sample mass due to the formation of bitumen.

In general, there is potential for altering the Mo, Zn and Cd isotopic compositions of the extracted rock residues if a sufficient fraction of isotopically distinct metal was removed along with the bitumen. Indeed, significant concentrations of Mo, Zn and Cd were found in the bitumen extracts (Fig. 5), in a similar vein to previous studies that have identified ug/g concentrations of Mo and in bitumens extracted from the Monterey Formation (Odermatt and Curiale, 1991), New Albany Shale (Mercer et al., 1992), Woodford Shale and Green River Shales (van Berkel, 1987) as well as in petroleum samples (Ventura et al., 2015).

The potential of metal fluid loss to alter the rock residue isotopic compositions can be quantified using simple mass-balance calculations of metals in the bulk rock and bitumen phases. Firstly, the fraction of each metal removed into the bitumen during each pyrolysis step can be calculated using the mass of the bitumen, along with the measured concentrations of metals in the bulk rock and the bitumen:

$$f_{Bit}^{X} = \frac{(f_{bit} * [X]_{bit})}{[X]_{rock}} \quad (2)$$

Where f_{Bit}^{X} is the fraction of metal X contained in the extracted bitumen, f_{bit} is the ratio of the mass of the bitumen to the mass of the starting rock (M_{Bit}/M_{Rock}), $[X]_{bit}$ is the concentration of the metal (Mo, Zn or Cd) in the extracted bitumen, and $[X]_{rock}$ is the concentration of Mo, Zn and Cd in the unextracted bulk rock. The results of these calculations are listed in Table 3. The fraction of Mo contained within the extracted bitumens range from 0.000–0.037 across the full range of maturity experiments for both the Kimmeridge Clay and the Posidonia Shale. The fractions of Zn contained within the extracted bitumens are slightly higher, ranging from 0.005–0.311. The fraction of Cd contained within extracted bitumens of both samples (0.001–0.205) is similar to Mo and Zn (Tables

3 and 4). Overall, in each experiment the fraction of each metal removed in bitumen is a small fraction of the total inventory of that metal in the rock.

The calculated bitumen metal fractions can be combined with their measured isotopic compositions to calculate the effect of fluid removal on the extracted rock residue isotopic compositions. The balance of mass in the experiments is:

$$f_{Rock}^{X} = f_{Bit}^{X} + f_{Res}^{X} + f_{Vol}^{X} \quad (3)$$

where f_{Vol} is the mass fraction of volatiles evolved and lost during pyrolysis. The isotope mass balance is:

$$f_{Rock}^{X}\delta_{Rock}^{X} = f_{Bit}^{X}\delta_{Bit}^{X} + f_{Res}^{X}\delta_{Res}^{X} \quad (4)$$

where $\delta_{Rock}^{X}, \delta_{Bit}^{X}, and\ \delta_{Res}^{X}$ are the isotope compositions of the bulk rock, bitumen, and extracted rock residue, respectively. If there was only minor volatile loss so that it can be assumed that f_{Vol}^{X}=0, then:

$$\delta_{Res}^{X} = \frac{\delta_{Rock}^{X} - \left(f_{Bit}^{X}\ \delta_{Bit}^{X}\right)}{1 - f_{Bit}^{X}} \quad (5)$$

As expected, the calculated rock residue $\delta^{98/95}$Mo values (1.84 ‰, varying only at the third decimal place) are always within uncertainty of measured non-pyrolysed bulk rock value of 1.84 ± 0.11 ‰. Although the bitumen fractions have isotopically light Zn signatures compared to bulk rocks (Fig 5), they contain relatively little Zn and thus result in calculated rock residue $\delta^{66/64}$Zn values of 0.45–0.52 ‰ that are the same as for the bulk rock (0.45 ± 0.05 ‰). Insufficient Cd in the bitumens prevented isotopic measurements, meaning that the Cd isotope composition of the extracted rock residues could not be calculated.

For Mo, the insignificant fractionation observed between bitumens and extracted rock residues means the removal of even large amounts of organically bound Mo would not induce a substantial isotopic change in the residue Mo. For Zn, where organic extracts are isotopically lighter than the extracted rock residues, ~10–30% of Zn would need to be removed into the bitumen to induce a >0.1 ‰ shift in the rock residue composition. Therefore, although there is a mobilisation of these metals by the bitumen fraction during pyrolysis, the fraction of metals transferred is not large enough for the isotopic composition of thermally matured mudrocks to be significantly altered. Consequently, useful paleo-depositional information may be retained in the isotopic compositions of thermally mature organic-rich mudrocks.

4.2 Changes in metal concentrations of rock residues

The increase in Mo, Zn and Cd concentrations and metal/TOC ratios with increasing maturity in the Kimmeridge and Posidonia experiments can be explained by a reduction in the mass of the bulk rock, which would act to concentrate the residual metals. This process would be expected to occur in view of the bitumen metal fractions that are always substantially less than in the residues, and in view of the combined loss of rock mass by bitumen removal, loss of volatile organic matter, and water from the dehydration of clays during heating,. The extent of this effect can be calculated:

$$C_{res} = \frac{C_{bulk}*(1-f_{bit-metal})}{1-f_{bit}} \quad (6)$$

Using the concentrations of Mo, Zn and Cd in the bulk rock samples as a starting point (C_{bulk}), calculated changes in metal concentrations capture the primary increases observed in the Kimmeridge Clay and Posidonia Shale rock residues (Fig. 7), albeit with some scatter, and thus support the contention that these increases are primarily driven by mass loss of the rock during catagenesis.

The substantial increase in metal concentrations observed in the experiments, replicated in two different types of starting rock, suggests that thermal maturation exerts a strong control on the metal concentrations, and on metal/TOC ratios of high maturity organic-rich mudrocks. This effect is not likely to adversely affect qualitative palaeoenvironmental interpretations using these proxies in single stratigraphic successions of limited spatial extent that experienced a common burial history. It is, however, likely to affect the detail of long-term reconstructions of metal inventories in global seawater across multi-million year timescales, which incorporate data from numerous different sections that may have experienced varying thermal and fluid migration histories (e.g. Scott et al., 2008, 2013; Partin et al., 2013; Sheen et al., 2018). In principle, a sedimentary host could retain its syn-depositional metal concentration if no fluid loss occurred. However, zero fluid loss would be extremely unlikely across burial-exhumation timescales of 10^7–10^9 years, and even harder to reject as a possibility from field data. The implication is that already very low Mo/TOC ratios previously documented from thermally mature euxinic successions (e.g. Algeo and Rowe, 2011), and indeed during the Proterozoic (Lyons et al., 2014) are likely to be upper estimates, with the 'true' syn-depositional concentrations perhaps as much as half those observed. Also, these new pyrolysis data suggest that the availability of bio-essential nutrients and oxygen inferred in these studies for past oceans may have been even lower than previously suggested from metal concentration data. Likewise, quantitative inferences of hydrographic situations inferred from the comparison of metal/TOC ratios in modern and ancient basins need to account for the thermal maturation of older sedimentary successions.

4.3 Distribution of Mo, Zn and Cd in organic matter

The similarity between the isotopic compositions of the bitumen and asphaltene fractions in Fig. 6 is consistent with the general observation that metals in organic fluids are primarily associated with

the asphaltene fraction (e.g. Yen, 1975; Duyck et al., 2008). Similar observations have also been made for rhenium and osmium in oils (Selby et al., 2007). It is generally observed that there is a decreasing metal concentration with maturation in oils, primarily because of the overall decrease in the asphaltene fraction at progressively higher maturities (Hitchon et al, 1975).

A wealth of previous pyrolysis studies have identified that asphaltenes and kerogens are structurally similar (Behar et al., 1984; Huc et al., 1984; Behar and Pelet, 1985; Eglinton et al., 1991; Horsfield et al., 1991; di Primio and Horsfield, 1996; Dieckmann et al., 2002;) and therefore that asphaltenes can be viewed as building blocks of the parent kerogen, cleaved off as high molecular weight fragments. In our study, we therefore assume that asphaltene ligands binding the trace metals in the bitumen are the same as those in the parent kerogens. Consequently, analysis of asphaltenes can be used to estimate the budgets of Mo, Zn and Cd associated with total organic matter. Note that organic matter has been measured in the bulk rocks as TOC, the concentration of organic carbon, while the concentration of organic matter is equal to [TOC] / $[C]_{OM}$. The fraction of the total budget of each metal in the bulk rock found in organic matter can be calculated using the metal concentration in the asphaltene extracts ($[X]_{asp}$) obtained from the early stages of pyrolysis (1 and 4 day experiments, prior to disproportionation of the asphaltenes to lower molecular weight compounds at higher maturities):

$$f_{OM}^{X} = \frac{[X]_{asp}[TOC]}{[X]_{Bulk}[C]_{OM}} \quad (7)$$

where f_{OM}^{X} is the fraction of metal X in the bulk rock organic matter, $[X]_{asp}$ and $[X]_{Bulk}$ are the concentrations of the metal in the asphaltene and bulk rock, respectively, and $[C]_{OM}$ is the concentration of C in the organic matter. This calculation shows that for the Kimmeridge Clay, only 4.5 ± 2.2 % of Mo, 12.4 ± 3.8 % of Zn and 8.1 ± 4.1 % of Cd is associated with organic matter (2 S.D. of n=4 asphaltene values). Similarly for the Posidonia Shale, only 2.6 % of Mo, 0.2 % of Zn and 3.6 % of Cd is associated with organic matter (n=1 asphaltene values, Fig. 8). The implication of Fig. 8 is that Mo and Zn, which are authigenically enriched over typical detrital contributions in these samples, are primarily held in inorganic phases, probably sulfides (Helz et al., 2011; Vance et al., 2016). There is insufficient data to determine if this is the case for Cd. Note that these values assume $[C]_{OM}$ = 1. An additional source of complexity in these estimates is that metals originally attached to inorganic particles may be bound to organic matter during diagenesis, or vice-versa. The data presented here cannot directly address this issue, but can be considered as maximum estimates of organically bound metals. These estimates provide a starting point for future studies to investigate the detailed partitioning of metals between organic and inorganic substrates.

The similarity between the Mo isotope composition of bulk rocks, bitumens asphaltenes and extracted rock residues in each rock is striking, and indicates that there is limited Mo isotopic fractionation during bitumen generation. This observation supports the contention that the Mo-isotope composition of oils reflects that of the source rock (Ventura et al., 2015). Therefore, based

on these experimental results, Mo-isotopes can be used for oil – source rock correlations with some confidence.

The Zn isotope composition of pyrolysate bitumens and asphaltenes are notably lighter than the bulk rocks by ~0.4–0.6 ‰. This observation raises the possibility that the isotopic composition of modern organic-rich sediments might be partly controlled by the presence of isotopically light Zn in organic matter itself. Alternatively, isotopically light Zn may be derived entirely from the burial of Zn-sulfides (Vance et al., 2016), which become diagenetically incorporated into organic matter following burial. The isotopically light signature of Zn in pyrolysed and non-pyrolysed bitumens and asphaltenes across the measured maturity gradient suggests that Zn-isotopes might also be used for oil – source rock bitumen correlations.

5. Conclusions

The starting point for the development of any geochemical proxy is a robust investigation of the processes that control its behaviour in the natural environment, in order to successfully disentangle useful palaeo-chemical signals from the rock record. The impact of catagenesis on the concentration of transition metals in ancient organic-rich mudrocks has rarely been studied (Mercer et al., 1992; van Berkel et al., 1987; Ardakani et al., 2017) and the impact of catagenesis on transition-metal isotope compositions has never been previously investigated. The results of laboratory pyrolysis experiments of two different organic-rich mudrocks presented here lead to a number of key conclusions:

(i) Catagenesis and the loss of volatile hydrocarbons does not induce changes in the Mo, Zn and Cd isotope compositions of the pyrolysed rock residues. This effect can be primarily attributed to the low partitioning of these metals into organic fluids, which results in a small total fractional loss of metals from the rock matrix. For Zn, where organic fluids are isotopically light compared to the bulk rock, approximately 10–30 % of the total zinc inventory would need to be transferred to organic fluids before the $\delta^{66/64}Zn$ of the bulk rock residue would change by >0.1 ‰.

(ii) Catagenesis leads to significant increases in the concentrations of Mo, Zn and Cd in the pyrolysed rock residues, and in corresponding element/TOC ratios. This effect can be attributed to a loss of mass during thermal maturation by the removal of bitumen and, coupled with the low partitioning of metals into organic fluids. Additional mass losses are probably due to the generation of H_2O, H_2S and CO_2 from both the organic and inorganic phases in the rocks. At high thermal maturities, Mo/TOC, Zn/TOC and Cd/TOC ratios may increase considerably. Consequently, the use of metal/TOC ratios in mature mudrock and shale deposits will lead to overestimates of dissolved metal inventories in the geological past.

(iii) The isotopic compositions of Mo and Zn in bitumens and asphaltenes are similar over the range of measured maturities. From this observation, it can be inferred that the solvent-extractable metal fraction is mainly bound to moieties within the asphaltenes.

(iv) The $\delta^{98/95}$Mo of bitumens are similar to the bulk rocks and rock residues, suggesting that $\delta^{98/95}$Mo can be used for oil to source rock correlations. In contrast, the $\delta^{66/64}$Zn of bitumens are generally 0.4–0.6 ‰ lighter than the bulk rocks and rock residues across the range of studied maturities, suggesting that Zn-isotopes may be used for oil to bitumen correlations.

(v) Several percent of the total metal inventory of Mo, Zn and Cd is directly associated with organic matter. This observation implies that inorganic constituents comprise the majority of the authigenic metal enrichments in these organic-rich mudrocks.

(vi) The results of this study constitute a first step towards understanding the effect of catagenesis on transition metal isotopes. It will be important for the results to be tested with more prolonged pyrolysis experiments, and in field-based studies.

Acknowledgements

We would like to thank Alan Hsieh and Phil Holdship for assistance with mass spectrometry, Steve Wyatt for helping with Soxhlet extractions and Jennifer Mabry for assistance with the vacuum line. Funding was provided by Shell Global Solutions B.V.

References

Abouchami, W., Galer, S.J.G., Horner, T.J., Rehkämper, M., Wombacher, F., Xue, Z., Lambelet, M., Gault-Ringold, M., Stirling, C.H., Schönbachler, M., Shiel, A.E., Weis, D. and Holdship, P.F. (2012), A common reference material for cadmium isotope studies – NIST SRM 3108. Geostandards and Geoanalytical Research doi: 10.1111/j.1751-908X.2012.00175.

Algeo, T.J. and Lyons, T.W. (2006), Mo-total organic carbon covariation in modern anoxic marine environments: implications for analysis of paleoredox and paleohydrologic conditions. *Paleoceanography* 21, PA1016, doi:10.1029/2004PA001112.

Algeo, T.J. and Rowe, H. (2012), Paleoceanographic applications of trace-metal concentration data. Chemical Geology 24, 6–18.

Algeo, T.J. and N. Tribovillard (2009), Environmental analysis of paleoceanographic systems based on molybdenum-uranium covariation. *Chem. Geol. 268*, 211-225.

Archer, C., Anderson, M.B., Cloquet, C., Conway, T.M., Dong, S., Ellwood, M., Moore, R., Nelson, J., Rehkämper, M., Rouxel, O., Samanta, M., Shin, K-C., Sohrin, Y., Takano, S. and Wasylenki, L.

(2016), Inter-calibration of a proposed new primary reference standard AA-ETH Zn, for zinc isotope analysis. Journal of Analytical Atomic Spectroscopy 32, 415–419.

Ardakani, O.H., Chappaz, A., Sanei, H. and Mayer, B. (2016), Effect of thermal maturity on remobilization of molybdenum in black shales. Earth and Planetary Science Letters 449, 311–320.

Arnold, G.L., Anbar, A.D., Barling, J. and Lyons, T.W. (2004), Molybdenum isotope evidence for widespread anoxia in the mid-Proterozoic oceans. *Science* 304, 87-90.

Asael, D., Tissot, F.L.H., Reinhard, C.T., Rouxel, O., Dauphas, N., Lyons, T.W., Ponzevera, E., Liorzou, C. and Chéron, S. (2013), Coupled molybdenum, iron and uranium stable isotopes as oceanic paleoredox proxies during the Paleoproterozoic Shunga event. Chemical Geology 362, 193–210.

Barling, J., Arnold, G.L. and Anbar, A.D. (2001), Natural mass-dependent variations in the isotopic composition of molybdenum. Earth and Planetary Science Letters 193, 447–457.

Behar, F., Beaumont, V. and Penteado, H.L.D.B. (2001), Rock-Eval 6: performances and developments. Oil and Gas Science and Technology 56, 111–134.

Behar, F. and Pelet, R. (1984), Characterisation of asphaltenes by pyrolysis and chromatography. Journal of Analytical and Applied Pyrolysis 7, 121–135.

Behar, F. and Pelet, R. (1985), Pyrolysis-gas chromatography applied to organic geochemistry: structural similarities between kerogens and asphaltenes from related rock extracts and oils. Journal of Analytical and Applied Pyrolysis 8, 173–187.

Behar, F., Pelet, R. and Roucache, J. (1984), Geochemistry of asphaltenes. Advances in Organic Geochemistry 1983. Pergamon, p587–595.

Brumsack, H-J. (1980), Geochemistry of Cretaceous black shales from the Atlantic Ocean (DSDP Legs 11, 14, 36 and 41). Chemical Geology 31, 1–25.

Chappaz, A., Lyons, T.W., Gregory, D.D., Reinhard, C.T., Gill, B.C., Li, C. and Large, R.R. (2014), Does pyrite act as an important host for molybdenum in modern and ancient euxinic sediments? Geochimica et Cosmochimica Acta 126, 112–122.

566 Dickson, A.J. (2017), A molybdenum isotope perspective on Phanerozoic deoxygenation events.
567 Nature Geoscience 10, 721–726.
568
569 Di Primio, R. and Horsfield, B. (1996), Predicting the generation of heavy oils in
570 carbonate/evaporitic environments using pyrolysis methods. Organic Geochemistry 24, 999–1016.
571
572 Dieckmann, V., Caccialanza, P.G. and Galimberti, R. (2002), Evaluating the timing of oil expulsion:
573 about the inverse behaviour of light hydrocarbons and oil asphaltene kinetics. Organic
574 Geochemistry 33, 1501–1513.
575
576 Duan, Y., Anbar, A.D., Arnold, G.L., Lyons, T.W., Gordon, G.W. and Kendall, B. (2010),
577 Molybdenum isotope evidence for mild environmental oxygenation before the Great Oxidation
578 Event. *Geochim. Cosmochim. Acta* 74, 6655-6668.
579
580 Duyck, C., Miekley, N., Fonseca, T.C.O., Szatmari, P. and Vaz dos Santos Neto, E. (2008), Trace
581 Element Distributions in Biodegraded Crude Oils and Fractions from the Potiguar Basin, Brazil.
582 Journal of the Brazil Chemical Society 19, 978–986.
583
584 Eglinton, T.I., Larter, S.R. and Boon, J.J. (1991), Characterisation of kerogens, coals and
585 asphaltenes by quantitative pyrolysis-mass spectrometry. Journal of Analytical and Applied
586 Pyrolysis 20, 25–45.
587
588 Ellrich, J., Hirner, A. and Stärk, H. (1985), Distribution of trace elements in crude oils from southern
589 Germany. Chemical Geology 48, 313–323.
590
591 Filby, R.H. (1994), Origin and nature of trace element species in crude oils, bitumens and
592 kerogens: implications for correlation and other geochemical studies. Geological Society of
593 London, Special Publications 78, 203–219.
594
595 Filby, R.H. and van Berkel,G.J. (1987), Geochemistry of metal complexes in petroleum source
596 rocks and coals: an overview. In: Filby, R.H. and Branthaver, J.F. (eds.), Metal complexes in fossil
597 fuels. American Chemical Society Symposium Series 344, 2–39.
598
599 Fitzgerald, S.L. and Filby, R.H. (1992), The effect of minerals on trace element distributions in
600 hydrous pyrolysates of kerogens from the New Albany Shale.
601

602 Georgiev, S.V., Horner, T.J., Stein, H.J., Hannah, J.L., Bingen, B. and Rehkämper, M. (2015),
603 Cadmium-isotopic evidence for increasing primary productivity during the Late Permian anoxic
604 event. Earth and Planetary Science Letters 410, 84–96.
605
606 Goldberg, T., Gordon, G., Izon, G., Archer, C., Pearce, C.R., McManus, J., Anbar, A.D. and
607 Rehkämper, M. (2013), Resolution of inter-laboratory discrepancies in Mo isotope data: an
608 intercalibration. *Journal of Analytical Atomic Spectrometry*, doi:10.1039/c3ja30375f.
609
610 Gordon, G.W., T.W. Lyons, G.L. Arnold, J. Roe, B.B. Sageman and A.D. Anbar (2009), When do
611 black shales tell molybdenum isotope tales? *Geology 37*, 535-538.
612
613 Helz, G.R., Miller, C.V., Charnock, J.M., Mosselmans, J.F.W., Pattrick, R.A.D., Garner, C.D. and
614 Vaughan, D.J. (1996), Mechanism of molybdenum removal from the sea and its concentration in
615 black shales: EXAFS evidence. Geochimica et Cosmochimica Acta 60, 3631–3642.
616
617 Helz, G.R., Bura-Nakić, E., Mikac, N. and Ciglenečki, I., 2011, New model for molybdenum
618 behaviour in euxinic waters. *Chem. Geol.* 284, 323-332.
619
620 Hitchon, B., Filby, R.H. and Shah, K.R. (1975), Geochemistry of trace elements in crude oils,
621 Alberta, Canada. In Yen, T.F. (ed.), The role of trace metals in petroleum. Ann Arbor Science
622 Publishers, Ann Arbor, USA, p111–122.
623
624 Horsfield, B., Heckers, J., Leythaeuser, D., Littke, R. and Mann, U. (1991), A study of the Holzener
625 Asphaltkalk, northern Germany: observations regarding the distribution, composition and origin of
626 organic matter in an exhumed petroleum reservoir. Marine and Petroleum Geology 8, 198–211.
627
628 Hu, Y-F. and Guo, T-M. (2001), Effect of temperature and molecular weight of n-alkane
629 precipitants on asphaltene precipitation. Fluid Phase Equilibria 192, 13–25.
630
631 Huc, A.Y., Behar, F. and Roussel, J.C. (1984), Geochemical variety of asphaltenes from crude oils:
632 characterisation of heavy crude oils and petroleum residue. Paris, Editions Technip 40, 99–103.
633
634 Janssen, D.J., Conway, T.M., John, S.G., Christian, J.R., Kramer, D.I., Pedersen, T.F. and Cullen,
635 J.T. (2014), Undocumented water column sink for cadmium in open ocean oxygen-deficient zones.
636 Proceedings of the National Academy of Sciences 111, 6888–6893.
637
638 Kendall, B., Dahl, T.W. and Anbar, A.D. (2017), Good goly, why moly? The stable isotope
639 geochemistry of molybdenum. Reviews in Mineralogy and Geochemistry 82, 683–732.

Lewan, M.D. (1984), Factors controlling the proportionality of vanadium to nickel in crude oils. Geochimica et Cosmochimica Acta 48, 2231–2238.

Lewan, M.D., Winters, J.C. and McDonald, J.H. (1979), Generation of oil-like pyrolysates from organic-rich shales. Science 203, 897–899.

Lewan, M.D. and Maynard, J.B. (1982), Factors controlling enrichment of vanadium and nickel in the bitumen of sedimentary rocks. Geochimica et Cosmochimica Acta 46, 2547–2560.

Little, S.H., Vance, D., McManus, J. and Severmann, S. (2016), Key role of continental margin sediments in the oceanic mass balance of Zn and Zn isotopes. Geology 44, 207–210.

Lyons, T.W., Reinhard, C.T. and Planavsky, N. (2014), The rise of oxygen in Earth's early ocean and atmosphere. Nature 506, 307–315.

McManus, J., T. Nägler, C. Siebert, C.G. Wheat and D.E. Hammond (2002), Oceanic molybdenum isotope fractionation: diagenesis and hydrothermal ridge-flank alteration. Geochemistry, Geophysics, Geosystems, 1078, doi:10.1029/2002GC0003569.

Mercer, G.E., Regner, A.J. and Filby, R.H. (1992), Trace element distributions in kerogen, bitumens and pyrolysates isolated from New Albany Shale. Preprints American Chemical Society Division of Fuel Chemistry 37, 1761–1768.

Mongenot, T., Tribovillard, N-P., Desprairies, A., Lallier-Vergès, E. and Laggoun-Defarge, F. (1996), Trace elements as palaeoenvironmental markers in strongly mature hydrocarbon source rocks: the Cretaceous La Luna formation of Venezuela. Sedimentary Geology 103, 23–37.

Morgans-Bell, H.S., Coe, A.L., Hesselbo, S.P., Jenkyns, H.C., Weedon, G.P., Marshall, J.E.A., Tyson, R.V. and Williams, C.J. (2001), Integrated stratigraphy of the Kimmeridge Clay Formation (Upper Jurassic) based on exposures and boreholes in south Dorset, UK. Geological Magazine 138, 511–539.

Nägler, T.F., Anbar, A.D., Archer, C., Goldberg, T., Gordon, G.W., Greber, N.D., Siebert, C., Sohrin, Y. and Vance, D. (2014), Proposal for an international molybdenum isotope measurement standard and data representation. Geostandards and Geoanalytical Research 38, 149–151.

677 Neubert, N., T.F. Nägler and M.E. Böttcher (2008), Sulphidity controls molybdenum isotope
678 fractionation into euxinic sediments: evidence from the modern Black Sea. Geology 36, 775-778.
679
680 Noordman, J., Weyer, S., Montoyo-Pina, C., Dellwig, O., Neubert, N., Eckert, S., Paetzel, M. amd
681 Bttcher, M.E. (2015), Uranium and molybdenum isotope systematics in modern euxinic basins:
682 case studies from the central Baltic Sea and the Kyllaren fjord (Norway). Chemical Geology 396,
683 182–195.
684
685 Odermatt, J.R. and Curiale, J.A. (1991), Organically bound metals and biomarkers in the Monterey
686 Formation of the Santa Maria Basin, California. Chemical Geology 91, 99–113.
687
688 Partin, C.A., Bekker, A., Planavsky, N.J., Scott, C.T., Gill, B.C., Li, C., Podkovyrov, V., Maslov, A.,
689 Konhauser, K.O., Lalonde, S.V., Love, G.D., Poulton, S.W. and Lyons, T.W. (2013), Large-scale
690 fluctuations in Precambrian atmospheric and oceanic oxygen levels from the record of U in shales.
691 Earth and Planetary Science Letters 369–370, 284–293.
692
693 Piper, D.Z and Calvert, S.E. (2009), A marine biogeochemical perspective on black shale
694 deposition. Earth Science Reviews 95, 63-96.
695
696 Poulson, R.L., C. Siebert, J. McManus and W.M. Berelson (2006), Authigenic molybdenum isotope
697 signatures in marine sediments, *Geology 34*, 617-620.
698
699 Poulson-Brucker, R.L., McManus, J., Severmann, S and Berelson, W.M. (2009), Molybdenum
700 behaviour during early diagenesis: insights from Mo isotopes. Geochemistry, Geophysics,
701 Geosystems 10, Q06010, doi:10.1029/2008GC002180.
702
703 Raiswell, R. and Berner, R.A. (1987), Organic carbon losses during burial and thermal maturation
704 of normal marine shales. Geology 15, 853–856.
705
706 Rooney, A.D., Selby, D., Lewan, M.D., Lillis, P.G. and Houzay, J-P. (2012), Evaluating Re-Os
707 systematics in organic-rich sedimentary rocks in response to petroleum generation using hydrous
708 pyrolysis experiments. Geochimica et Cosmochimica Acta 77, 275–291.
709
710 Scotchman, I.C. (1990), Kerogen facies and maturity of the Kimmeridge Clay Formation in
711 southern and eastern England. Marine and Petroleum Geology 8, 278–295.
712
713 Scott, C., T.W. Lyons, Bekker, A., Shen, Y., Poulton, S.W., Chu, X. and Anbar, A.D. (2008),
714 Tracing the stepwise oxygenation of the Proterozoic ocean. Nature 452, 456–459.

Scott, C., Planavsky, N.J., Dupont, C.L., Kendall, B., Gill, B.C., Robbins, L.J., Husband, K.F., Arnold, G.L., Wing, B.A., Poulton, S.W., Bekker, A., Anbar, A.D., Konhauser, K.O. and Lyons, T.W. (2013), Bioavailability of zinc in marine systems through time. Nature Geoscience 6, 125–128.

Selby, D., Creaser, R.A. and Fowler, M.G. (2007), Re-Os elemental and isotopic systematics in crude oils. Geochimica et Cosmochimica Acta 71, 378–386.

Siebert, C., Nägler, T.F., von Blanckenburg, F. and Kramers, J.D. (2003), Molybdenum isotope records as a potential new proxy for paleoceanography, *Earth Planet. Sci. Lett. 211*, 159-171.

Siebert, C., J. McManus, A. Bice, R. Poulson and W.M. Berelson (2006), Molybdenum isotope signatures in continental margin sediments, *Earth Planet. Sci. Lett. 241,* 723-733.

Sweere, T., van den Boorn, S., Dickson, A.J. and Reichart, G-J. (2016), Definition of new trace-metal proxies for the controls on organic matter enrichment in marine sediments based on Mn, Co, Mo and Cd concentrations. Chemical Geology 441, 235–245.

Tissot, B.P. and Welte, D.H. (1984), Petroleum formation and occurrence. Springer, Berlin, Heidelberg.

Tribovillard, N., Algeo, T.J., Lyons, T. and Riboulleau, A. (2006), Trace metals as paleoredox and paleoproductivity proxies: an update. *Chem. Geol.* 232, 12-32.

van Berkel,G.J. (1987), The role of kerogen in the evolution of the nickel and vanadyl porphyrins. PhD dissertation, Washington State University, Pullman, WA.

Vance, D., Little, S.H., Archer, C., Cameron, V., Andersen, M.B., Rijkenberg, M. and Lyons, T.W. (2016), The oceanic budgets of nickel and zinc isotopes: the importance of sulfidic environments as illustrated by the Black Sea. Philosophical Transactions of the Royal Society A374, 20150296, doi:10.1098/rsta.2015.0294.

Ventura, G.T., Gall, L., Siebert, C., Prytulak, J., Szatmari, P., Hürlimann, M. and Halliday, A.N. (2015), The stable isotope composition of vanadium, nickel, and molybdenum in crude oils. Applied Geochemistry 59, 104–117.

Wille, M., Nägler, T.F., Lehmann, B., Schröder, D. and Kramers, J.D. (2008), Hydrogen sulphide release to surface waters at the Precambrian/Cambrian boundary. *Nature* 435, 767-769.

Yen, T. F. (1975), The role of trace metals in petroleum. Ann Arbor Science Publishers, Ann Arbor, USA, pp.219.

Figure captions

Figure 1: The changing proportions of the different organic matter constituents in a sample as thermal maturation progresses. Kerogen is the solid organic matter that remains after mainly microbial diagenesis in near-surface sediments, and which progressively breaks down into fluid-phase organic matter (bitumen) during catagenic alteration. This process yields a rising proportion of bitumen throughout maturation, which in a natural system would be prone to migration away from the host rock. At the highest stages of maturation, any bitumen that does not migrate can be re-incorporated into the solid fraction again as pyro-bitumen.

Figure 2: Overview of the experimental procedures and analytical approach. Operational terms are defined in the text.

Figure 3: Bulk organic geochemical results. A: Heating time versus T_{max}. B: Heating time versus hydrogen index (HI). C: Heating time versus %TOC. D: Heating time versus transformation ratio $[(HI_{original} - HI_{measured})/HI_{original}]$. Filled symbols are for the Posidonia Shale, and open symbols are for the Kimmeridge Blackstone Band. Uncertainties are the 2 S.D. of sample aliquots measured in triplicate. Dashed lines indicate trends in the datasets.

Figure 4: Mo, Zn and Cd isotopes, concentrations, and metal/TOC ratios for bulk rocks and rock residues of the Kimmeridge Blackstone Band and the Posidonia Shale. Horizontal lines indicate the mean values of the bulk rock and rock residue isotope data across the measured maturity ranges, and the 2 S.D. external reproducibilities. Individual uncertainties for isotope data points are the propagated 2 S.E. of the measurements and the bracketing zero-delta standards.

Figure 5: Mo, Zn and Cd isotopes and concentrations for bitumens and asphaltenes of the Kimmeridge Blackstone Band and the Posidonia Shale. Horizontal lines show the mean values of the bulk rock and rock residue isotope data across the measured maturity ranges, and the 2 S.D. external reproducibilities, for comparison. Individual uncertainties for isotope data points are the propagated 2 S.E. of the measurements and the bracketing zero-delta standards. Grey bands indicate the range of metals concentrations measured in bulk rocks and extracted rock residues.

Figure 6: Comparison between Mo and Zn isotope and concentration data for extracted pyrolysate bitumens and asphaltenes.

Figure 7: Comparison between measured molybdenum and zinc concentrations in bulk rocks and rock residues, with predicted concentrations calculated from equation (6).

Figure 8: Organic-matter bound Mo, Zn and Cd in the Kimmeridge Blackstone Band (A) and in the Posidonia Shale (B) expressed as a percentage of the total rock metal inventory. Values were calculated using equation (7).

Table 1: Kimmeridge Blackstone Band geochemical data. HI: hydrogen index. TOC: total organic carbon. T_{max}: temperature of maximum hydrocarbon yield during pyrolysis. TR: transformation ratio (change in hydrogen index during pyrolysis). Ext. Res: extracted residue, i.e. pyrolysed bulk rock after solvent extraction of soluble organic matter. Bitumen: the total solvent-extractable organic matter. Asphalt: asphaltene fraction, i.e. the *n*-heptane insoluble fraction of the bitumen. N.D.: not determined.

Heating time (hours)	Sample type	HI	TOC (%)	T_{max} (^{o}C)	TR	Al (ppm)	$\delta^{98/95}$Mo (‰)	2 S.E.	Mo (ppm)	$\delta^{66/64}$Zn (‰)	2 S.E.	Zn (ppm)	$\delta^{114/110}$Cd (‰)	2 S.E.	Cd (ppm)	Mo/TOC (x10^{-4})	Zn/TOC (x10^{-4})	Cd/TOC (x10^{-4})
0	Bulk rock	733	35.2	413	0	21220	1.84	0.11	47.02	0.45	0.05	37.3	0.26	0.13	1.10	1.34	1.06	0.031
0 (#1)	Ext. Res.	715	35.0	412	0.02	25330	n.d.	n.d.	n.d.	n.d.	n.d.	n.d.	n.d.	n.d.	n.d.	n.d.	n.d.	n.d.
	Bitumen	n.d.	n.d.	n.d.	n.d.	240	2.05	0.03	2.35	0.04	0.02	27.10	n.d.	n.d.	0.08	n.d.	n.d.	n.d.
	Asphalt.	n.d.	n.d.	n.d.	n.d.	200	2.06	0.03	5.83	-0.08	0.04	67.17	n.d.	n.d.	0.11	n.d.	n.d.	n.d.
0 (#2)	Ext. Res.	725	34.8	413	0.01	24610	1.83	0.11	49.29	0.41	0.06	37.92	0.12	0.10	0.97	1.42	1.09	0.028
	Bitumen	n.d.	n.d.	n.d.	n.d.	170	1.99	0.03	4.40	-0.13	0.19	9.52	n.d.	n.d.	0.09	n.d.	n.d.	n.d.
	Asphalt.	n.d.	n.d.	n.d.	n.d.	140	2.02	0.03	4.20	-0.11	0.05	9.47	n.d.	n.d.	0.12	n.d.	n.d.	n.d.
24 (#1)	Ext. Res.	685	36.8	414	0.07	14710	1.89	0.04	52.41	0.34	0.08	47.24	n.d.	n.d.	n.d.	1.42	1.28	n.d.
	Bitumen	n.d.	n.d.	n.d.	n.d.	4970	1.73	0.03	10.70	-0.36	0.04	268.44	n.d.	n.d.	0.39	n.d.	n.d.	n.d.
	Asphalt.	n.d.	n.d.	n.d.	n.d.	3910	1.83	0.05	9.87	-0.39	0.04	287.24	n.d.	n.d.	0.39	n.d.	n.d.	n.d.
24 (#2)	Ext. Res.	719	36.0	413	0.02	23170	1.87	0.04	52.80	0.51	0.05	58.60	n.d.	n.d.	0.95	1.47	1.63	0.026
	Bitumen	n.d.	n.d.	n.d.	n.d.	2090	1.73	0.06	3.05	0.26	0.07	8.56	n.d.	n.d.	0.19	n.d.	n.d.	n.d.
	Asphalt.	n.d.	n.d.	n.d.	n.d.	1960	1.78	0.05	4.93	0.27	0.06	15.60	n.d.	n.d.	0.30	n.d.	n.d.	n.d.
96 (#1)	Ext. Res.	665	35.2	417	0.09	27590	1.89	0.04	56.15	0.41	0.07	57.31	n.d.	n.d.	n.d.	1.60	1.63	n.d.
	Bitumen	n.d.	n.d.	n.d.	n.d.	670	1.84	0.03	3.81	0.58	0.10	8.54	n.d.	n.d.	0.14	n.d.	n.d.	n.d.
	Asphalt.	n.d.	n.d.	n.d.	n.d.	2160	1.80	0.03	4.47	0.40	0.08	10.27	n.d.	n.d.	0.16	n.d.	n.d.	n.d.
96 (#2)	Ext. Res.	665	35.8	418	0.09	15580	1.86	0.02	55.52	0.41	0.06	116.54	n.d.	n.d.	1.05	1.55	3.26	0.029
	Bitumen	n.d.	n.d.	n.d.	n.d.	620	1.77	0.03	4.67	-0.11	0.07	79.32	n.d.	n.d.	0.13	n.d.	n.d.	n.d.
	Asphalt.	n.d.	n.d.	n.d.	n.d.	570	1.79	0.03	3.92	-0.23	0.05	74.27	n.d.	n.d.	0.13	n.d.	n.d.	n.d.
325 (#1)	Ext. Res.	510	31.4	433	0.30	19690	1.85	0.02	65.89	0.44	0.06	54.88	n.d.	n.d.	1.18	2.10	1.75	0.037
	Bitumen	n.d.	n.d.	n.d.	n.d.	34	1.92	0.04	4.03	-0.67	0.12	9.71	n.d.	n.d.	0.08	n.d.	n.d.	n.d.
	Asphalt.	n.d.	n.d.	n.d.	n.d.	n.d.	1.93	0.04	n.d.	-0.81	0.07	n.d.	n.d.	n.d.	n.d.	n.d.	n.d.	n.d.
325 (#2)	Ext. Res. #1	521	31.7	432	0.29	26310	1.85	0.02	67.56	0.43	0.07	52.53	0.14	0.09	1.20	2.13	1.66	0.038
	Ext. Res. #2	n.d.	n.d.	n.d.	n.d.	n.d.	n.d.	n.d.	n.d.	n.d.	n.d.	n.d.	0.40	0.09	1.44	n.d.	n.d.	0.045
	Bitumen	n.d.	n.d.	n.d.	n.d.	8	1.94	0.04	3.06	-0.72	0.04	23.59	n.d.	n.d.	0.08	n.d.	n.d.	n.d.
	Asphalt.	n.d.	n.d.	n.d.	n.d.	28	1.91	0.03	5.63	-0.72	0.03	44.39	n.d.	n.d.	0.11	n.d.	n.d.	n.d.
840 (#1)	Ext. Res.	178	33.0	451	0.76	40920	1.84	0.04	69.91	0.46	0.04	54.72	n.d.	n.d.	n.d.	2.12	1.66	n.d.
	Bitumen	n.d.	n.d.	n.d.	n.d.	320	1.72	0.40	0.09	2.43	0.07	1.48	n.d.	n.d.	0.90	n.d.	n.d.	n.d.
	Asphalt.	n.d.	n.d.	n.d.	n.d.	12	1.72	0.12	0.18	0.17	0.06	1.84	n.d.	n.d.	0.03	n.d.	n.d.	n.d.

Table 2: Posidonia Shale geochemical data. Definitions of terms are the same as for table 1.

Heating time (hours)	Sample type	HI	TOC (%)	T_{max} (^{o}C)	TR	Al (ppm)	$\delta^{98/95}$Mo (‰)	2 S.E.	Mo (ppm)	$\delta^{66/64}$Zn (‰)	2 S.E.	Zn (ppm)	$\delta^{114/110}$Cd (‰)	2 S.E.	Cd (ppm)	Mo/TOC (x10^{-4})	Zn/TOC (x10^{-4})	Cd/TOC (x10^{-4})
0	Bulk rock	702	12.89	432	0	26030	1.58	0.04	123.56	0.51	0.03	242.54	0.03	0.07	2.63	9.59	18.82	0.20
0	Ext. Res.	706	11.72	432	0	30660	1.57	0.02	121.88	0.54	0.04	195.15	0.02	0.05	2.39	10.40	16.65	0.20
	Bitumen	n.d.	n.d.	n.d.	n.d.	120	1.17	0.14	0.95	0.05	0.03	17.86	n.d.	n.d.	0.07	n.d.	n.d.	n.d.
	Asphalt.	n.d.	n.d.	n.d.	n.d.	100	1.46	0.03	1.68	0.01	0.03	33.06	n.d.	n.d.	0.09	n.d.	n.d.	n.d.
96	Ext. Res.	589	9.97	436	0.16	30560	1.61	0.04	124.87	0.51	0.04	293.92	0.08	0.11	2.59	12.52	29.48	0.26
	Bitumen	n.d.	n.d.	n.d.	n.d.	1090	1.47	0.04	9.59	0.15	0.03	24.75	n.d.	n.d.	0.21	n.d.	n.d.	n.d.
	Asphalt.	n.d.	n.d.	n.d.	n.d.	n.d.	1.51	0.03	31.83	0.13	0.03	93.48	n.d.	n.d.	0.75	n.d.	n.d.	n.d.
840	Ext. Res.	239	7.42	442	0.66	32280	1.58	0.04	131.49	n.d.	n.d.	n.d.	0.05	0.04	3.11	17.73	n.d.	0.42
	Bitumen	n.d.	n.d.	n.d.	n.d.	45	1.33	0.24	2.19	n.d.	n.d.	n.d.	n.d.	n.d.	0.05	n.d.	n.d.	n.d.
	Asphalt.	n.d.	n.d.	n.d.	n.d.	59	1.52	0.04	5.29	0.08	0.04	25.48	n.d.	n.d.	0.13	n.d.	n.d.	n.d.

Table 3: Calculated changes in rock residue metal concentrations and isotope compositions in the Kimmeridge Blackstone Band. Uncertainties in the calculated isotope compositions of the rock residues are propagated through equation (5), assuming conservative 2% uncertainties for isotope dilution concentrations and 5% uncertainties for sample masses.

Heating time (hours)	% total rock mass of extracted bitumen	Fraction of Mo in bitumen	Calculated bulk residue Mo (ppm)	Calculated bulk residue $\delta^{98/95}$Mo (‰)	Propagated uncertainty (‰)	Fraction of Zn in bitumen	Calculated bulk residue Zn (ppm)	Calculated bulk $\delta^{66/64}$Zn (‰)	Propagated uncertainty (‰)	Fraction of Cd in bitumen	Calculated bulk residue Cd (ppm)
0	2.4	0.001	48.1	1.84	0.15	0.017	37.6	0.46	0.04	0.002	1.12
0	2.1	0.002	47.9	1.84	0.15	0.005	37.9	0.45	0.04	0.002	1.12
24	16.4	0.037	54.1	1.84	0.15	n.d.	n.d.	n.d.	n.d.	0.058	1.24
24	10.8	0.007	52.3	1.84	0.15	0.025	40.8	0.46	0.04	0.019	1.21
96	6.5	0.005	50.0	1.84	0.15	0.015	39.3	0.45	0.04	0.009	1.17
96	14.6	0.015	54.3	1.84	0.15	0.311	30.1	0.70	0.06	0.018	1.27
325	22.0	0.019	59.1	1.84	0.15	0.057	45.1	0.52	0.04	0.017	1.39
325	7.3	0.005	50.5	1.84	0.15	0.046	38.4	0.51	0.04	0.005	1.18
840	25.0	0.000	62.6	1.84	0.15	0.010	49.2	0.43	0.03	0.205	1.17

Table 4: Calculated changes in rock residue metal concentrations and isotope compositions in the Posidonia Shale. Uncertainties in the calculated isotope compositions of the rock residues are propagated as for Table 3.

Heating time (hours)	% total rock mass of extracted bitumen	Fraction of Mo in bitumen	Calculated bulk residue Mo (ppm)	Calculated bulk residue $\delta^{98/95}$Mo (‰)	Propagated uncertainty (‰)	Fraction of Zn in bitumen	Calculated bulk residue Zn (ppm)	Calculated bulk $\delta^{66/64}$Zn (‰)	Propagated uncertainty (‰)	Fraction of Cd in bitumen	Calculated bulk residue Cd (ppm)
0	4.2	0	128.9	1.58	0.13	0.003	252.9	0.51	0.04	0.001	2.7
96	4.1	0.003	128.5	1.58	0.13	0.004	252.1	0.51	0.04	0.003	2.7
840	20.8	0.004	155.4	1.58	0.13	n.d.	305.0	0.51	0.04	0.004	3.3

Figure

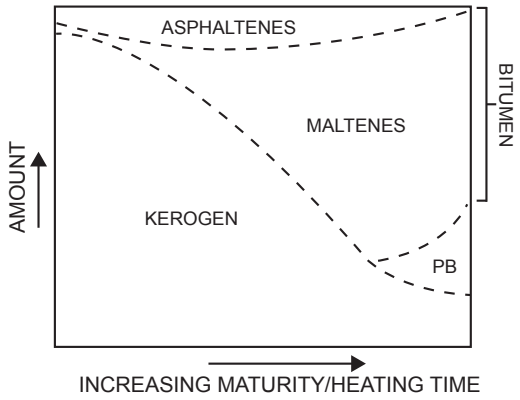
ASPHALTENES
MALTENES
KEROGEN
PB
BITUMEN
AMOUNT
INCREASING MATURITY/HEATING TIME

Figure

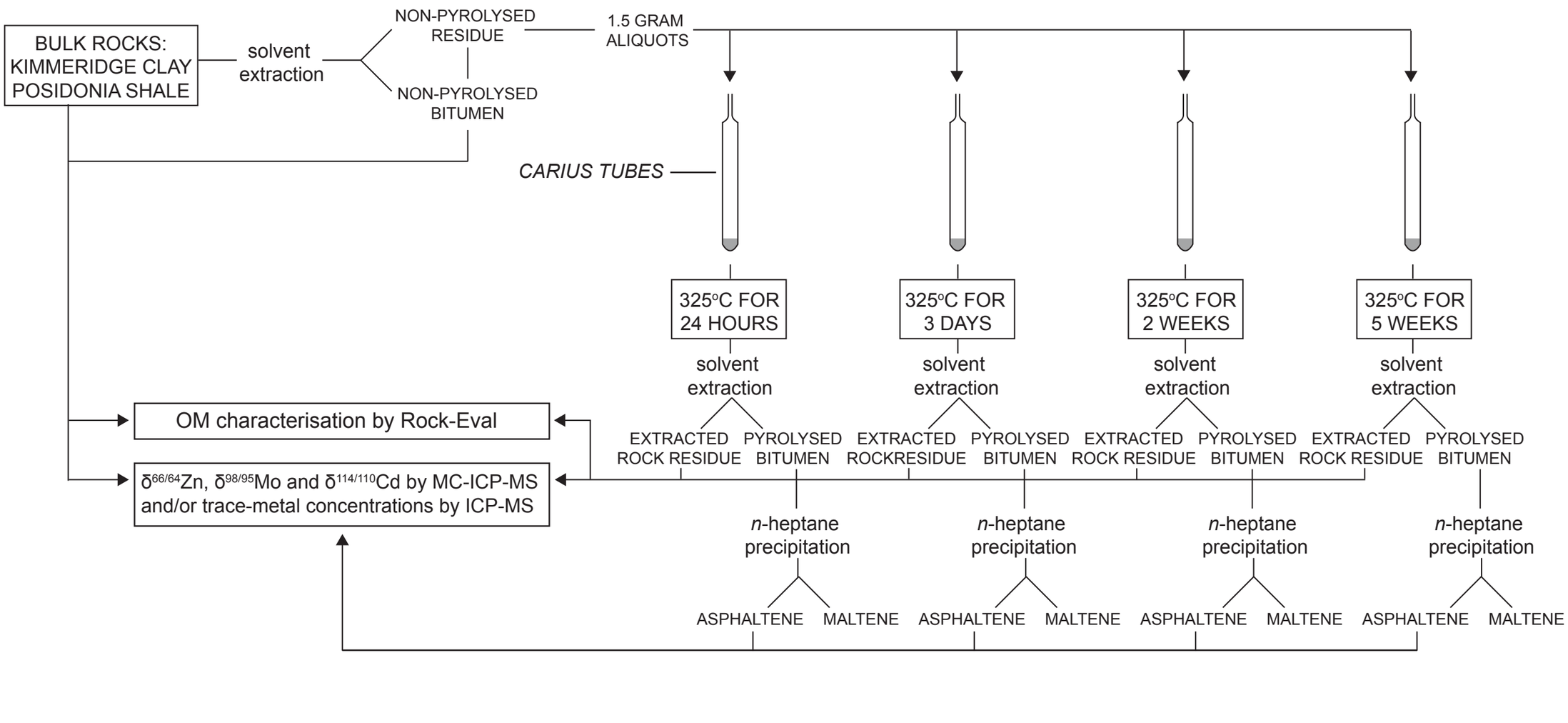
BULK ROCKS: KIMMERIDGE CLAY POSIDONIA SHALE
solvent extraction
NON-PYROLYSED RESIDUE
NON-PYROLYSED BITUMEN
1.5 GRAM ALIQUOTS
CARIUS TUBES
325°C FOR 24 HOURS
325°C FOR 3 DAYS
325°C FOR 2 WEEKS
325°C FOR 5 WEEKS
solvent extraction
solvent extraction
solvent extraction
solvent extraction
OM characterisation by Rock-Eval
δ66/64Zn, δ98/95Mo and δ114/110Cd by MC-ICP-MS and/or trace-metal concentrations by ICP-MS
EXTRACTED ROCK RESIDUE
PYROLYSED BITUMEN
EXTRACTED ROCKRESIDUE
PYROLYSED BITUMEN
EXTRACTED ROCK RESIDUE
PYROLYSED BITUMEN
EXTRACTED ROCK RESIDUE
PYROLYSED BITUMEN
n-heptane precipitation
n-heptane precipitation
n-heptane precipitation
n-heptane precipitation
ASPHALTENE
MALTENE
ASPHALTENE
MALTENE
ASPHALTENE
MALTENE
ASPHALTENE
MALTENE

Figure

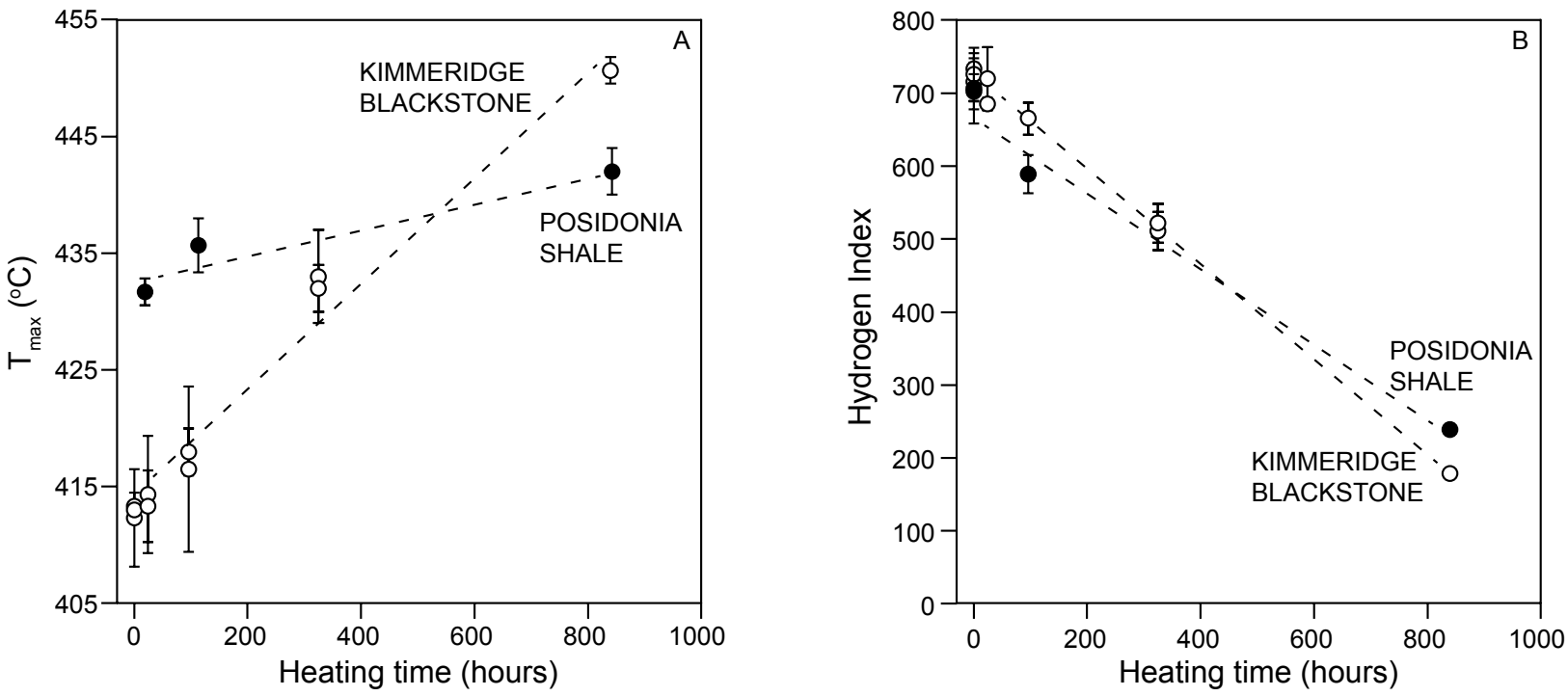
A
KIMMERIDGE
BLACKSTONE
POSIDONIA
SHALE
T_{max} (°C)
Heating time (hours)
B
Hydrogen Index
POSIDONIA
SHALE
KIMMERIDGE
BLACKSTONE
Heating time (hours)
C
KIMMERIDGE
BLACKSTONE
POSIDONIA
SHALE
TOC (%)
Heating time (hours)
D
KIMMERIDGE
BLACKSTONE
POSIDONIA
SHALE
Transformation ratio
Heating time (hours)

Figure

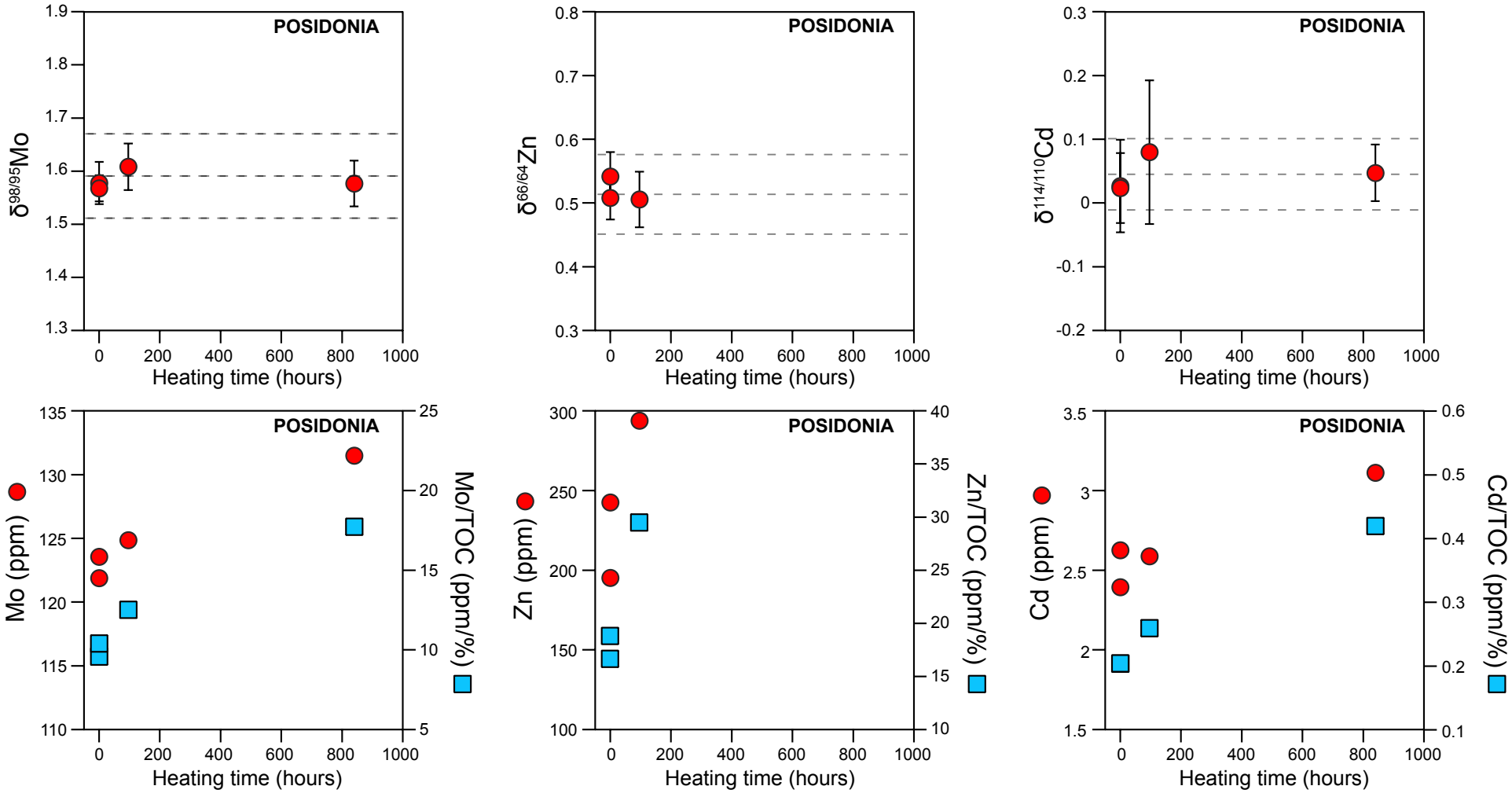
POSIDONIA
δ98/95Mo
δ66/64Zn
δ114/110Cd
Mo (ppm)
Mo/TOC (ppm/%)
Zn (ppm)
Zn/TOC (ppm/%)
Cd (ppm)
Cd/TOC (ppm/%)
Heating time (hours)
KIMMERIDGE
δ98/95Mo
δ66/64Zn
δ114/110Cd
Mo (ppm)
Mo/TOC (ppm/%)
Zn (ppm)
Zn/TOC (ppm/%)
Cd (ppm)
Cd/TOC (ppm/%)
Heating time (hours)

Figure

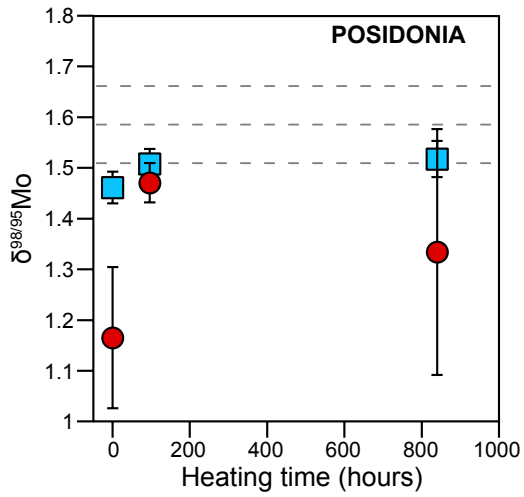
POSIDONIA
δ98/95Mo
Heating time (hours)

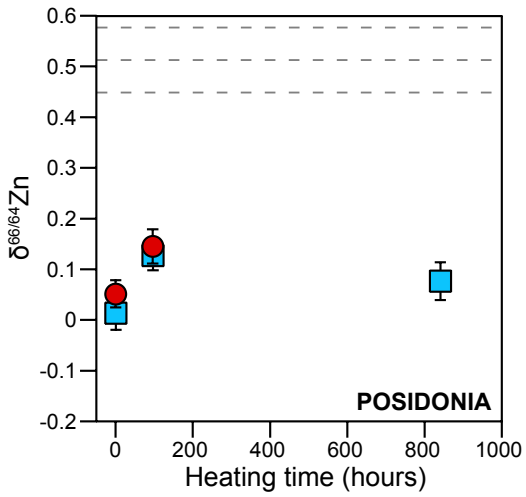
POSIDONIA
δ66/64Zn
Heating time (hours)

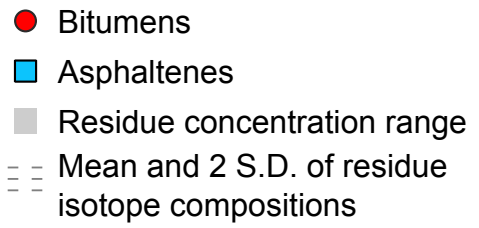
Bitumens
Asphaltenes
Residue concentration range
Mean and 2 S.D. of residue isotope compositions

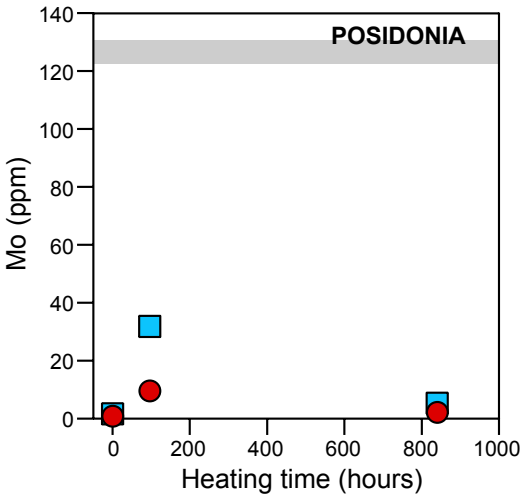
POSIDONIA
Mo (ppm)
Heating time (hours)

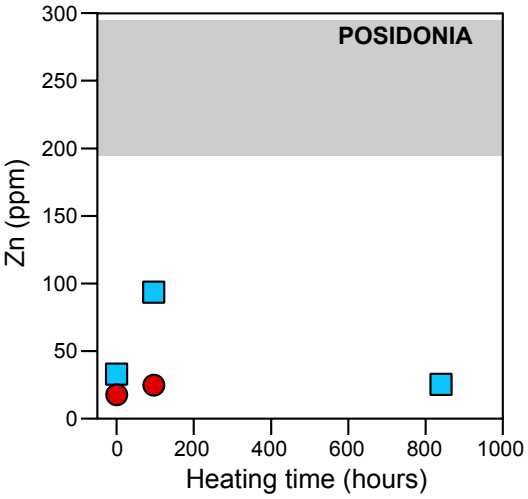
POSIDONIA
Zn (ppm)
Heating time (hours)

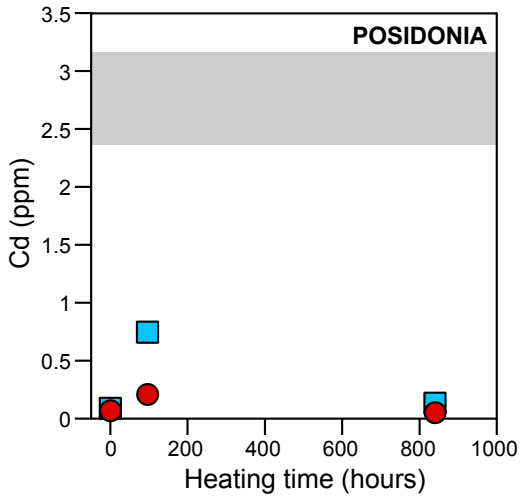
POSIDONIA
Cd (ppm)
Heating time (hours)

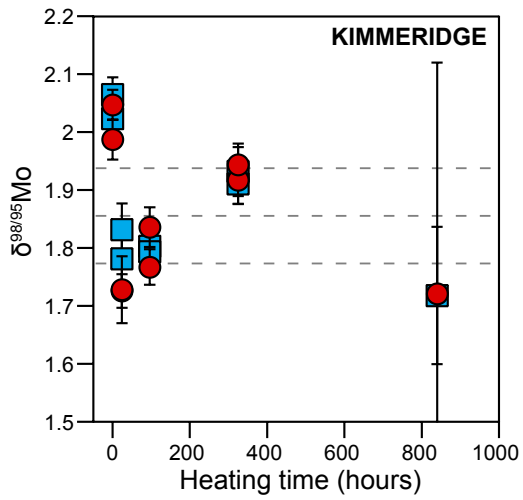
KIMMERIDGE
δ98/95Mo
Heating time (hours)

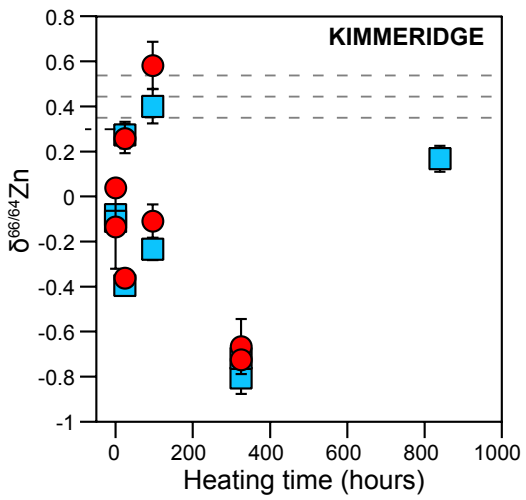
KIMMERIDGE
δ66/64Zn
Heating time (hours)

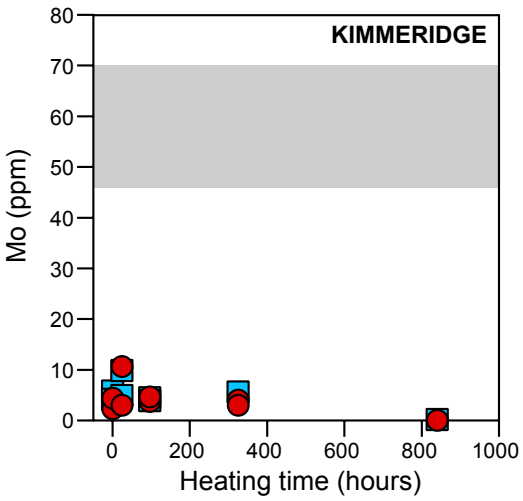
KIMMERIDGE
Mo (ppm)
Heating time (hours)

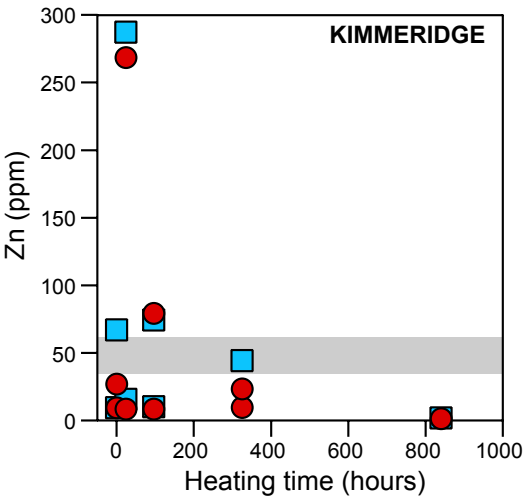
KIMMERIDGE
Zn (ppm)
Heating time (hours)

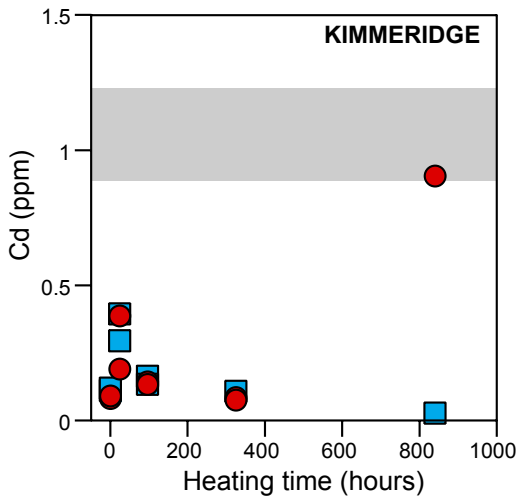
KIMMERIDGE
Cd (ppm)
Heating time (hours)

Figure

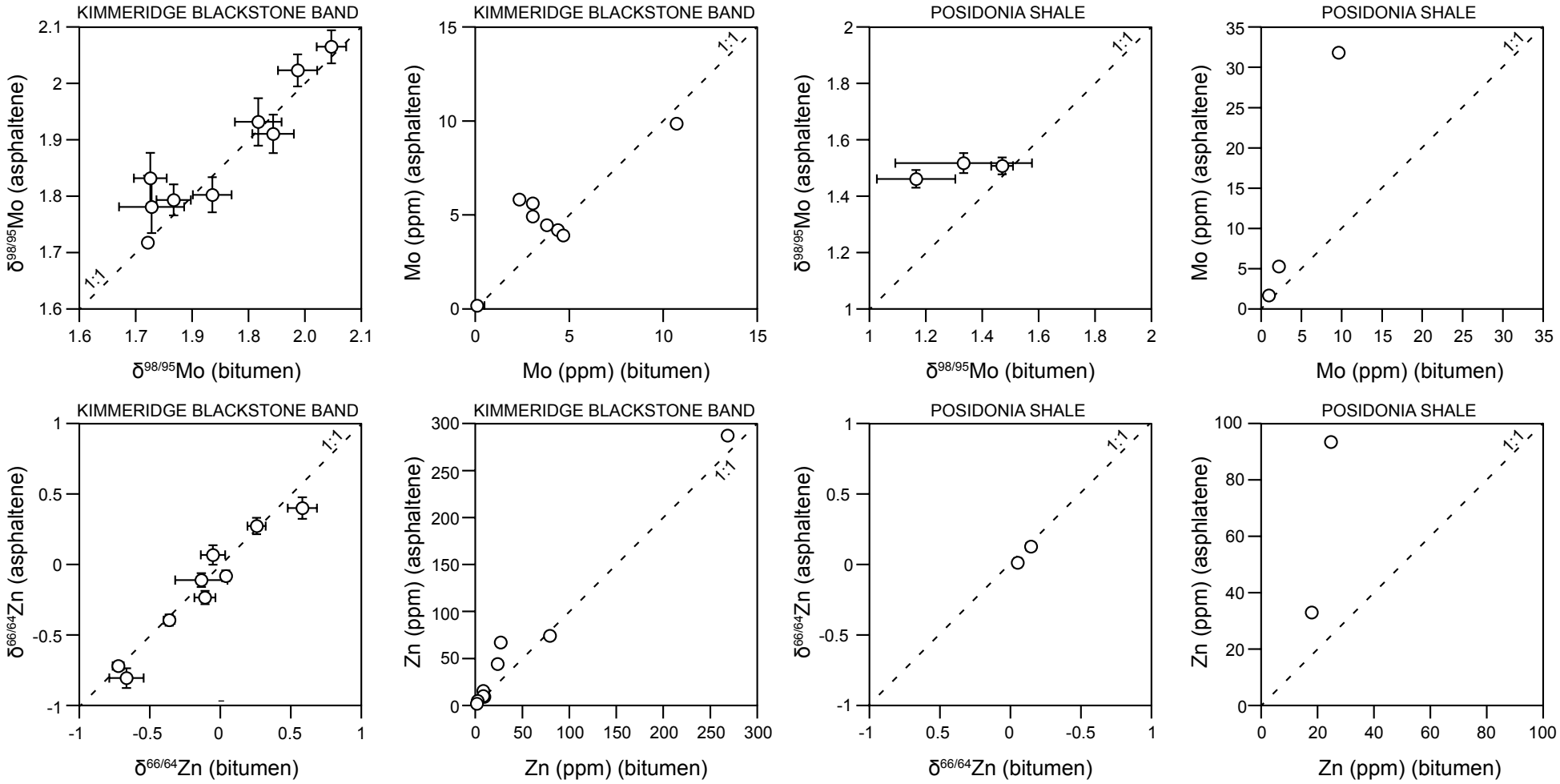
KIMMERIDGE BLACKSTONE BAND
δ98/95Mo (asphaltene)
δ98/95Mo (bitumen)
1:1
KIMMERIDGE BLACKSTONE BAND
Mo (ppm) (asphaltene)
Mo (ppm) (bitumen)
1:1
POSIDONIA SHALE
δ98/95Mo (asphaltene)
δ98/95Mo (bitumen)
1:1
POSIDONIA SHALE
Mo (ppm) (asphaltene)
Mo (ppm) (bitumen)
1:1
KIMMERIDGE BLACKSTONE BAND
δ66/64Zn (asphaltene)
δ66/64Zn (bitumen)
1:1
KIMMERIDGE BLACKSTONE BAND
Zn (ppm) (asphaltene)
Zn (ppm) (bitumen)
1:1
POSIDONIA SHALE
δ66/64Zn (asphaltene)
δ66/64Zn (bitumen)
1:1
POSIDONIA SHALE
Zn (ppm) (asphlatene)
Zn (ppm) (bitumen)
1:1

Figure

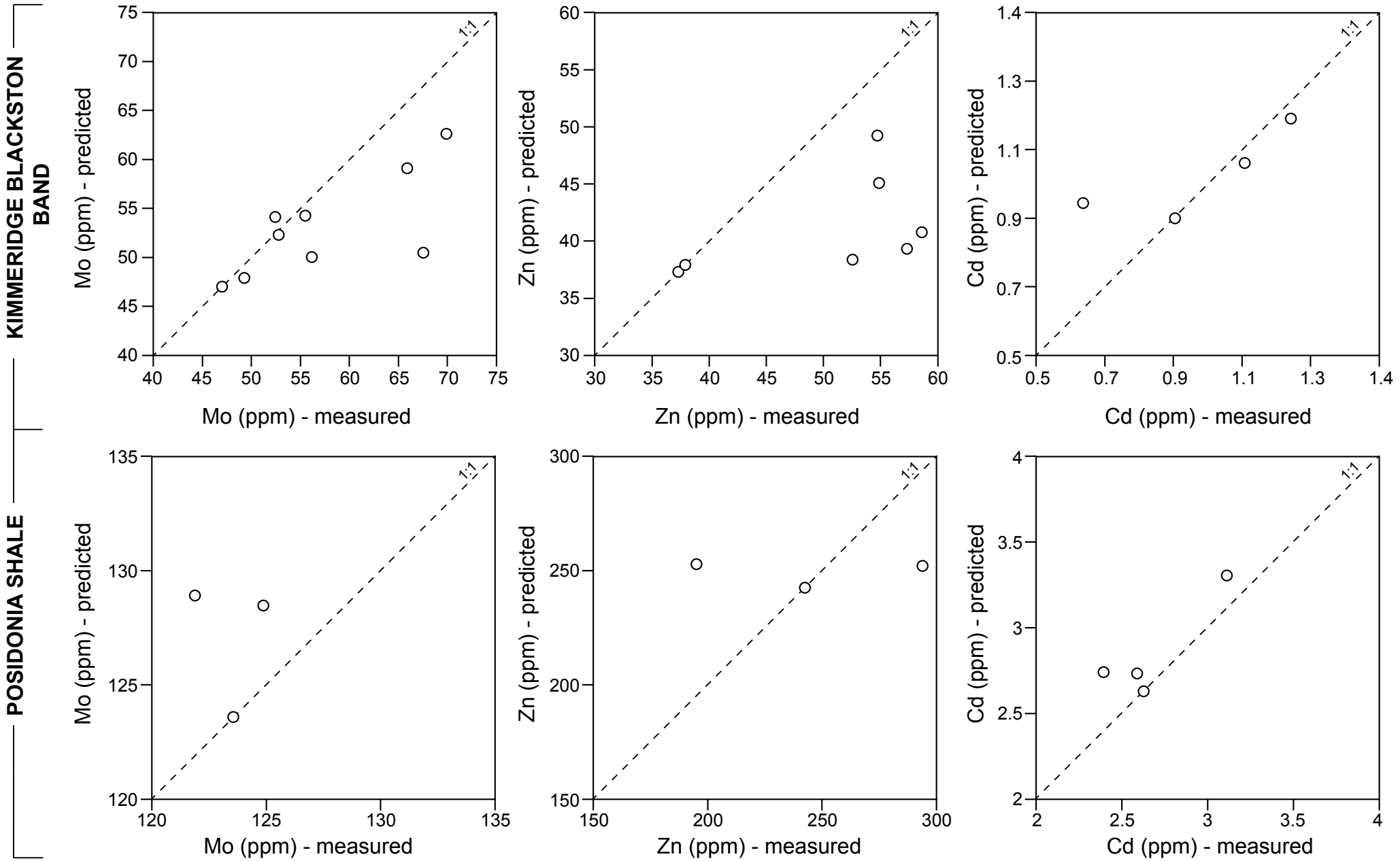
KIMMERIDGE BLACKSTON BAND
POSIDONIA SHALE
Mo (ppm) - predicted
Mo (ppm) - measured
Zn (ppm) - predicted
Zn (ppm) - measured
Cd (ppm) - predicted
Cd (ppm) - measured
1:1

Figure

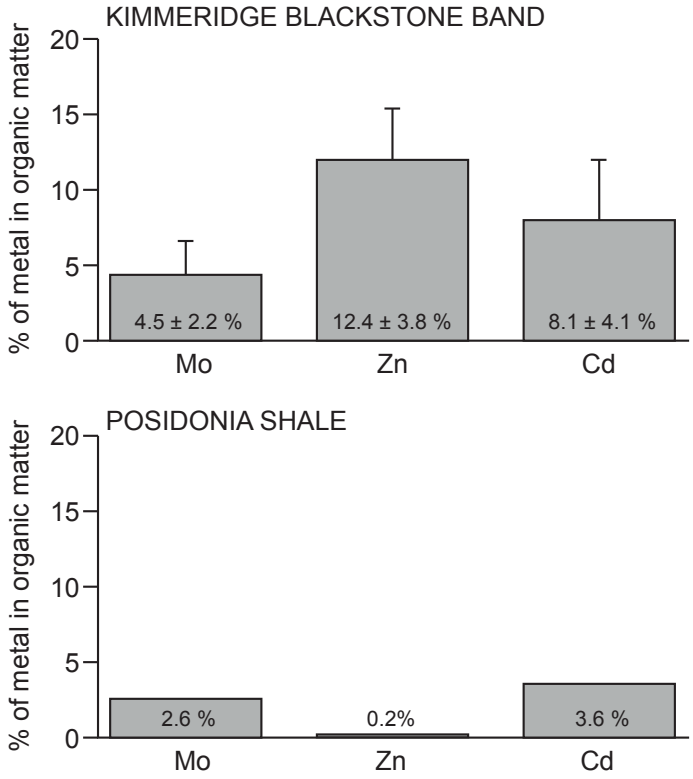
KIMMERIDGE BLACKSTONE BAND
% of metal in organic matter
20
15
10
5
0
4.5 ± 2.2 %
12.4 ± 3.8 %
8.1 ± 4.1 %
Mo
Zn
Cd
POSIDONIA SHALE
% of metal in organic matter
20
15
10
5
0
2.6 %
0.2%
3.6 %
Mo
Zn
Cd

Source or Other Companion File

Click here to download Source or Other Companion File: Pyrolysis manuscript_REVISED2_TC__August2019.docx